

Metadata of the article that will be visualized in OnlineFirst

ArticleTitle	Characterization and comparison of natural and Zachery-treated turquoise: new data	
--------------	------------------------------------------------------------------------------------	--

Article Sub-Title		
-------------------	--	--

Article CopyRight	The Author(s), under exclusive licence to Springer-Verlag GmbH Germany, part of Springer Nature (This will be the copyright line in the final PDF)	
-------------------	-------------------------------------------------------------------------------------------------------------------------------------------------------	--

Journal Name	Physics and Chemistry of Minerals	
--------------	-----------------------------------	--

Corresponding Author	FamilyName	Diella
	Particle	
	Given Name	Valeria
	Suffix	
	Division	Institute of Environmental Geology and Geoengineering (IGAG)
	Organization	National Research Council, Section of Milan
	Address	Via Botticelli 23, 20133, Milan, Italy
	Phone	
	Fax	
	Email	valeria.diella55@gmail.com
	ORCID	http://orcid.org/0000-0001-8767-9164

Author	FamilyName	Cantaluppi
	Particle	
	Given Name	Marco
	Suffix	
	Division	Department of Earth Sciences "Ardito Desio"
	Organization	University of Milan
	Address	Via Botticelli 23, 20133, Milan, Italy
	Phone	
	Fax	
	Email	marco.cantaluppi@unimi.it
	ORCID	http://orcid.org/0000-0002-3914-6491

Author	FamilyName	Bocchio
	Particle	
	Given Name	Rosangela
	Suffix	
	Division	Department of Earth Sciences "Ardito Desio"
	Organization	University of Milan
	Address	Via Botticelli 23, 20133, Milan, Italy
	Phone	
	Fax	
	Email	rosangela.bocchio@unimi.it
	ORCID	http://orcid.org/0000-0002-8635-0874

Author	FamilyName	Possenti
	Particle	
	Given Name	Elena
	Suffix	
	Division	Institute of Heritage Science (ISPC)
	Organization	National Research Council, Section of Milan
	Address	Via R. Cozzi 53, 20125, Milan, Italy
	Phone	
	Fax	
	Email	elena.possenti@cnr.it
	ORCID	http://orcid.org/0000-0002-9041-7971

Author	FamilyName	Adamo
	Particle	
	Given Name	Ilaria
	Suffix	
	Division	
	Organization	Italian Gemmological Institute (IGI)
	Address	Piazza S. Sepolcro 1, 20123, Milan, Italy
	Phone	
	Fax	
	Email	ilaria.adamo@igi.it
	URL	
	ORCID	

Author	FamilyName	Ventura
	Particle	
	Given Name	Giancarlo Della
	Suffix	
	Division	Department of Sciences
	Organization	University of Rome Tre
	Address	Largo S. Leonardo Murialdo 1, 00146, Rome, Italy
	Phone	
	Fax	
	Email	giancarlo.dellaventura@uniroma3.it
	URL	
	ORCID	http://orcid.org/0000-0001-6277-961X

Author	FamilyName	Mancini
	Particle	
	Given Name	Lucia
	Suffix	
	Division	
	Organization	Elettra-Sincrotrone Trieste S.C.P.A.
	Address	S.S. 14 Km 163, 500 in Area Science Park, 34149, Basovizza (Trieste), Italy
	Phone	
	Fax	
	Email	lucia.mancini@elettra.eu
	URL	
	ORCID	

Author	FamilyName	Marinoni
	Particle	
	Given Name	Nicoletta
	Suffix	
	Division	Department of Earth Sciences “Ardito Desio”
	Organization	University of Milan
	Address	Via Botticelli 23, 20133, Milan, Italy
	Phone	
	Fax	
	Email	nicoletta.marinoni@unimi.it
	URL	
	ORCID	http://orcid.org/0000-0003-4969-4923

Schedule	Received	22 Apr 2022
	Revised	
	Accepted	17 May 2023

Abstract

Turquoise is a well-known gemstone that has been used in artefacts across many cultures throughout history. However, due to its porosity it is often treated to enhance its color and beauty. One appreciated treatment is the patented Zachery process, although its details remain publicly undisclosed. Previous studies indicated that only a high K content distinguishes Zachery-treated from natural turquoises. In this study, natural and Zachery-treated turquoise samples from the famous Kingman mine, Arizona, USA, were analysed by means a multi-methodological approach, including standard gemological testing, electron microprobe (EMPA), scanning electron microscope with energy dispersive spectrometer (SEM-EDS) and X-ray diffraction (XRD), Fourier-Transform InfraRed (FTIR), non-destructive External Reflection-Fourier-Transform InfraRed (ER-FTIR) spectroscopy and X-ray computed microtomography (μ CT). The results revealed new chemical-mineralogical and microstructural features that distinguish the Zachery-treated from the natural turquoise: higher specific gravity and lower porosity, associated with high and uneven concentrations of Cu, K and Na, the occurrence of tenorite (CuO), the presence and extension of reaction edges in the entire volume are distinctive of treated samples. Moreover, Cu-rich seeds and feldspar crystals may be interpreted as additional components used during the treatment. The hypothesis is that the Zachery treatment induces the re-crystallization of a new turquoise-like phase, which differs from the natural one from a chemical and microstructural point of view.

Keywords (separated by '- ') Turquoise - Gemology - Zachery method - FTIR and ER-FTIR spectroscopy - Chemical analyses - X-ray computed microtomography

Footnote Information



2 Characterization and comparison of natural and Zachery-treated 3 turquoise: new data

4 Valeria Diella¹ · Marco Cantaluppi² · Rosangela Bocchio² · Elena Possenti³ · Ilaria Adamo⁴ ·
5 Giancarlo Della Ventura⁵ · Lucia Mancini⁶ · Nicoletta Marinoni²

6 Received: 22 April 2022 / Accepted: 17 May 2023

7 © The Author(s), under exclusive licence to Springer-Verlag GmbH Germany, part of Springer Nature 2023

8 Abstract

AQ1 Turquoise is a well-known gemstone that has been used in artefacts across many cultures throughout history. However, due to its porosity it is often treated to enhance its color and beauty. One appreciated treatment is the patented Zachery process, although its details remain publicly undisclosed. Previous studies indicated that only a high K content distinguishes Zachery-treated from natural turquoises. In this study, natural and Zachery-treated turquoise samples from the famous Kingman mine, Arizona, USA, were analysed by means a multi-methodological approach, including standard gemological testing, electron microprobe (EMPA), scanning electron microscope with energy dispersive spectrometer (SEM-EDS) and X-ray diffraction (XRD), Fourier-Transform InfraRed (FTIR), non-destructive External Reflection-Fourier-Transform InfraRed (ER-FTIR) spectroscopy and X-ray computed microtomography (μ CT). The results revealed new chemical–mineralogical and microstructural features that distinguish the Zackery-treated from the natural turquoise: higher specific gravity and lower porosity, associated with high and uneven concentrations of Cu, K and Na, the occurrence of tenorite (CuO), the presence and extension of reaction edges in the entire volume are distinctive of treated samples. Moreover, Cu-rich seeds and feldspar crystals may be interpreted as additional components used during the treatment. The hypothesis is that the Zachery treatment induces the re-crystallization of a new turquoise-like phase, which differs from the natural one from a chemical and microstructural point of view.

23 **Keywords** Turquoise · Gemology · Zachery method · FTIR and ER-FTIR spectroscopy · Chemical analyses · X-ray
24 computed microtomography

A1 ✉ Valeria Diella
A2 valeria.diella55@gmail.com

A3 Marco Cantaluppi
A4 marco.cantaluppi@unimi.it

A5 Rosangela Bocchio
A6 rosangela.bocchio@unimi.it

A7 Elena Possenti
A8 elena.possenti@cnr.it

A9 Ilaria Adamo
A10 ilaria.adamo@igi.it

A11 Giancarlo Della Ventura
A12 giancarlo.dellaventura@uniroma3.it

A13 Lucia Mancini
A14 lucia.mancini@elettra.eu

A15 Nicoletta Marinoni
A16 nicoletta.marinoni@unimi.it

1 Institute of Environmental Geology and Geoengineering (IGAG), National Research Council, Section of Milan, Via Botticelli 23, 20133 Milan, Italy A17 A18 A19

2 Department of Earth Sciences “Ardito Desio”, University of Milan, Via Botticelli 23, 20133 Milan, Italy A20 A21

3 Institute of Heritage Science (ISPC), National Research Council, Section of Milan, Via R. Cozzi 53, 20125 Milan, Italy A22 A23 A24

4 Italian Gemmological Institute (IGI), Piazza S. Sepolcro 1, 20123 Milan, Italy A25 A26

5 Department of Sciences, University of Rome Tre, Largo S. Leonardo Murialdo 1, 00146 Rome, Italy A27 A28

6 Elettra-Sincrotrone Trieste S.C.P.A., S.S. 14 Km 163, 500 in Area Science Park, 34149 Basovizza (Trieste), Italy A29 A30

25 Introduction

26 The main purpose of the activity of gemologists is the
 27 evaluation of gem materials, that is establishing their iden-
 28 tity and determining whether they are natural or synthetic
 29 and/or if they have been treated (Fritsch and Rondeau
 30 2009). The term “*Treatment*” refers to any artificial pro-
 31 cess, different from cut and assembly, used to improve the
 32 gem color, appearance, and durability. All stones, even
 33 artificial ones, can be subjected to treatments, which must
 34 be explicitly declared as such (Shigley and McClure 2009).
 35 In the past, some treatments were not disclosed but gener-
 36 ally accepted; one example is the fracture filling with oil
 37 of emerald, a treatment that is no longer accepted unless
 38 it is disclosed.

39 Turquoise, with chemical formula
 40 $\text{CuAl}_6(\text{PO}_4)_4(\text{OH})_8 \cdot 4\text{H}_2\text{O}$, is one of the first gem materi-
 41 als that has been subjected to various methods of treat-
 42 ments to improve its appearance and mechanical proper-
 43 ties and consequently to increase the amount available
 44 and its commercial value. The ancient use of turquoise
 45 in jewelry dates back to the beginning of civilization,
 46 from ancient Persia (7000 B.C.) and Egypt (5000 B.C.)
 47 to the present day (Hole et al. 1969; Carò et al. 2021 and
 48 references therein). Turquoise occurs in dry and barren
 49 regions where acidic, copper-rich groundwater reacts with
 50 minerals containing phosphorous and aluminium and is
 51 found in large amounts in Iran, China, Mexico, Australia
 52 and in southwestern part of the USA, mainly in Nevada
 53 and Arizona (Schwarzinger and Schwarzinger 2017 and
 54 reference therein). However, in most cases, the sources
 55 of high-quality gem samples are limited and unsatisfac-
 56 tory for the demand of the market. Moreover, turquoise,
 57 being a cryptocrystalline aggregate with various degrees
 58 of porosity, can easily accept many treatments. The most
 59 common type of turquoise treatment is the impregnation
 60 with organic material, such as polymers and wax, which
 61 improves the durability and appearance of the gemstone
 62 (Fritsch et al. 1999; McClure et al. 2010). The distinc-
 63 tion of natural, untreated turquoise from its counterpart
 64 by impregnation requires a combination of standard gemo-
 65 logical observations with more sophisticated techniques,
 66 mainly Raman and Fourier-transform infrared (FTIR)
 67 spectroscopy, chemical analyses, X-ray diffraction, and
 68 analytical pyrolysis (Lind et al. 1983; Fritsch et al. 1999;
 69 McClure et al. 2010; Čejka et al. 2015; Schwarzinger and
 70 Schwarzinger 2017; Sabbaghi 2018; Dumanska-Slowik
 71 et al. 2020).

72 Since 1988, a new proprietary type of turquoise treat-
 73 ment, called “Zachery treatment” has appeared on the
 74 market (Fritsch et al. 1999 and references therein). The
 75 treatment greatly enhances the stone’s quality and aspect

76 preserving its gemological properties, decreasing its
 77 porosity, improving its color, and allowing easier polish-
 78 ing. Fritsch et al. (1999) published a thorough paper on
 79 this proprietary process highlighting the difficulties to
 80 recognize the treated turquoises by standard gemologi-
 81 cal techniques and assessing that this treatment does not
 82 involve any impregnation with a polymer. In that paper, the
 83 Zachery method is described as a process involving a bath
 84 of mineral fragments under a flux of electrical current.
 85 Fritsch et al. (1999) claimed that the enhancement process
 86 is based on the attempts to duplicate the environment that
 87 allowed the famous Kingman high-grade turquoise to be
 88 deposited amid large potassium feldspar beds and that the
 89 procedure, including the electrodes controlling the cur-
 90 rent flux, did not contain colouring ions such as iron and
 91 copper. The Authors concluded that only the exposition to
 92 oxalic acid that bleach the stone or chemical analysis that
 93 detects the presence of potassium, found in most Zach-
 94 ery-treated turquoises, may identify the treatment. Fur-
 95 ther studies on Zachery-treated turquoises (Kwon et al.
 96 2009; Sun et al. 2014) reiterated that only the high content
 97 of potassium could be used to distinguish natural from
 98 treated stones.

99 The present study characterizes and compares natural and
 100 Zachery-treated turquoise by a multidisciplinary approach
 101 combining either non-destructive or invasive methods. The
 102 research has a dual purpose: first to clarify the Zachery treat-
 103 ment, which is still undisclosed and, second, to provide dis-
 104 tinctive features that facilitate the easy and rapid recognition
 105 of treated samples.

106 The non-destructive techniques on cut samples, regard-
 107 less of their size, include gemological investigation, External
 108 Reflection-Fourier-Transform InfraRed (ER-FTIR) spectro-
 109 scopy, and X-ray computed microtomography (μCT) whereas
 110 chemical analyses by Electron Microprobe (SEM-Q), scan-
 111 ning electron microscope with energy dispersive spectrom-
 112 eter (SEM-EDS), analyses by X-ray diffraction (XRD) and
 113 Fourier-Transform InfraRed (FTIR) spectroscopy imply loss
 114 or damage of the samples.

115 Materials and methods

116 A group of 31 gem-quality turquoises from the Kingman
 117 mine (Arizona, USA), 14 natural and 17 Zachery-treated,
 118 provided by the Italian Gemological Institute (IGI) thanks
 119 to Dr. Claudio Cimmino, Bangkok, Thailandia, were inves-
 120 tigated using different techniques to characterize their mor-
 121 phological and chemical features. In the following, *TN* and
 122 *TT* will refer to natural and treated turquoises, respectively.

123 Five natural (*TN_1-5*) and six treated (*TT_1-6*) gems
 124 were tested by standard gemological methods at the Italian
 125 Gemological Institute of Milan (Italy) to determine their

gemological properties. Three treated samples (*TT_1-3*) were sawed in half to investigate their cross sections. The samples weighing from 1.51 to 7.87 ct are fashioned as cabochons or spheres. Their refractive index, n , was measured by the spot method with a Krüss refractometer (A. Krüss Optronic, Hamburg, Germany) using an ordinary light source with a sodium filter (wavelength $\lambda = 589$ nm) and methylene iodide as a contact liquid ($n = 1.80$). A Mettler hydrostatic balance was used to determine the specific gravity (SG) in bi-distilled water. We also examined the reaction of the samples to both the long-wave ($\lambda = 366$ nm) and short-wave ($\lambda = 245$ nm) ultraviolet radiation in a darkened room. Moreover, a Motic GM168 dark-field gemological microscope was used for the microscopic observations.

Quantitative chemical analyses of major and minor elements were performed and backscattered electron (BSE) images acquired on the polished surface of three natural specimens (*TN_6*, *TN_7* and *TN_8*), on the polished surface of a treated one (*TT_7*) and on two perpendicularly cut treated specimens (*TT_8* and *TT_9*) using the JEOL JXA-8200 electron microprobe in wavelength dispersion mode (EMPA-WDS) at the Department of Earth Sciences of the University of Milan, Italy. The system was operated with an accelerating voltage of 15 kV, 5 nA beam current and a counting time of 60 s on the peak and 30 s on the background selecting a 10 μm diameter spot to prevent the sample sublimation under the electron beam. Natural minerals were used as standards and the rough data were corrected for matrix effects using a conventional $\Phi\rho Z$ routine in the JEOL software package.

At the same laboratories, a further investigation was performed using the Scanning Electron Microscope (SEM) JSM-IT 500 (JEOL, 2019), equipped with an Energy Dispersive Spectrometer (EDS), to obtain X-ray maps, secondary and backscattered electron (SE and BSE) images at high magnification and rapid semi-quantitative analyses. Twelve samples, 2 natural (*TN_9-10*) and 10 treated (*TT_10-19*), have been coated with gold for secondary electron images or carbon for BSE images, semi-quantitative chemical analyses, and X-ray maps.

Five fragments (two natural, *TN_12-13*, and three treated, *TT_21-23*) were selected for powder X-ray diffraction measurements. The analyses were performed at the Department of Earth Sciences of the University of Milan, Italy, by a Panalytical X'Pert-PROMPD X'Celerator X-ray powder diffractometer, using Cu K α radiation ($\lambda = 1.5418$ Å), at a beam voltage of 40 kV and a current of 40 mA. X-ray powder diffraction patterns were collected over the 9–120° range of the scattering angle 2θ , with steps of 0.01° 2θ and a count time of 50 s per step. The lattice parameters of the turquoise samples were determined by using Si (NBS SRM 640b) as an internal standard and the General Structure Analysis System

(GSAS) software was used to process XRD data (Rietveld 1969; Toby and Dreele 2013).

Infrared spectroscopy measurements were carried out on natural and treated turquoises with two different instrumental setups (powder FTIR and External Reflection FTIR) described below. The aim was to explore the vibrational features of the gems and the potentials of the two IR approaches in detecting the differences between the natural and treated turquoises. External reflection FTIR is a relatively little-exploited but efficient method to identify minerals and gems (Hainschwang and Notari 2008).

The Powder FTIR spectra were collected at the laboratory of the Department of Sciences, University of Rome Tre, Italy, on one natural (*TN_14*) and three treated (*TT_24-26*) turquoises using a Nicolet iS50 FTIR spectrometer equipped with a DTGS detector and a KBr beam splitter in a spectral range of 4000–400 cm^{-1} ; the nominal resolution was 4 cm^{-1} and 64 scans were averaged for both samples and background. Small fragments were manually extracted under the binocular microscope from the pristine and treated turquoise, respectively, based on the different blue hue of the sample and the distance from the rim of the gemstone, that was affected by the treatment. The fragments were ground using an agate mortar, mixed with KBr (mineral:KBr ratio = 1:200 mg) and pressed to prepare the conventional KBr disks for IR transmission analysis.

External reflection Fourier transform infrared spectroscopy (ER-FTIR) measurements were carried out on one natural (*TN_15*) and two treated turquoises (*TT_20* and *TT_27*) using a Thermo Scientific™ Nicolet™ iS50 FT-IR spectrophotometer coupled with a Continuum™ infrared microscope equipped with a mercury cadmium telluride (MCT/A) detector cooled with liquid nitrogen and located at the laboratory of the Institute of Heritage Science (ISPC-CNR), Milan, Italy. The investigations were performed non-invasively in specular reflectance geometry, in the spectral range 4000–650 cm^{-1} , with a 4 cm^{-1} resolution and by merging 128 co-added scans. The background spectra were collected on a golden mirror. The investigated area was 100 \times 100 μm^2 for each ER-FTIR spectrum. ER-FTIR measurements were done on the external surface of the gems and along the traverse from rim to centre. In the following, the ER-FTIR spectra are presented in reflectance without any spectral manipulation or spectral conversion.

Laboratory-based X-ray computed microtomography (μCT) analyses of two cut turquoises, one natural (*TN_11*) and one treated (*TT_20*), were performed at the TomoLab station (Mancini et al. 2007; Zandomenighi et al. 2010; Kudrna Prašek et al. 2018; Caruso et al. 2020) of the Elettra synchrotron facility in Basovizza (Trieste, Italy). This μCT system is equipped with a sealed microfocus X-ray source (L9181, Hamamatsu Photonic, Japan) operating in a Voltage range of 40–130 kV with a maximum power of 39 W,

a minimum focal spot size of 5 μm and delivering an X-ray beam with a cone beam geometry. The detector used was a 12-bit, water-cooled, full-frame CCD camera (4008 × 2672 pixels) coupled to a Gadox scintillator screen by a fiber-optic taper. This camera has an effective pixel size of 12.5 × 12.5 mm² corresponding to a maximum field of view of 50 × 33 mm². The experimental parameters used for the tomographic scans are the followings: Voltage = 130 kV, current = 61 μA, angular step = 0.2°, total scan angle = 360°, scan duration = 174 min, scaled pixel size = 5 μm). The slice reconstruction was carried out using the free software Necon 1.7 (Bruker, USA) based on the Feldkamp algorithm (Feldkamp et al. 1984), which also allows us to correct beam hardening and ring artefacts. The visualization of the reconstructed virtual section of the samples was obtained by the freeware ImageJ, while for the 3D visualization (rendering) of the virtual volumes, the commercial software VGStudio Max 2.0 (Volume Graphics, Germany) was applied.

Image segmentation, aimed at extracting the pores/cracks from the matrix, has been performed by manual 3D Otsu thresholding using the Fiji software (Schindelin et al. 2012) and the results are reported as pore volume percentage (% vol).

Results

Gemological properties

The samples range in color from whitish or greenish light blue to dark blue. In general, the treated samples have darker and more saturated colors, unnatural in appearance, when compared with their untreated counterparts, which appear whitish or greenish light blue in color. Moreover, the luster of the treated stones is better than that of untreated samples which show a chalky luster (Fig. 1).

For all samples, the refractive index ranges from 1.60 to 1.62 (spot method), in agreement with literature data (Fritsch et al. 1999). The measured specific gravity (SG) of natural untreated stones ranges from 2.44 to 2.57 g/cm³ and increases from about 5 up to 15% after about a quarter of an hour immersed in water. The treated samples have no tendency to absorb water and their SG results in the range from 2.65 to 2.74 g/cm³. This confirms that the untreated turquoise samples are more porous than their treated counterparts.

All samples (both untreated and treated) are inert to short-wave UV and show a weak to very weak whitish blue or whitish green luminescence to long-wave irradiation. When viewed with the gemological microscope, all untreated samples reveal a typical turquoise structure with cavities, whitish spots and yellow inclusions having metallic luster (pyrite). The treated samples are more homogeneous in their

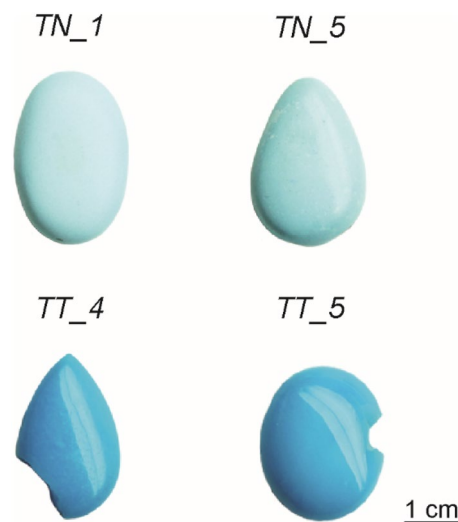


Fig. 1 Examples of studied turquoises: *TN_1*: 11.18 × 17.43 × 5.22 mm, 7.867 ct; *TN_5*: 9.89 × 13.61 × 4.39 mm, 4.29 ct; *TT_4*: 7.87 × 13.18 × 2.44 mm, 1.67 ct; *TT_5*: 7.89 × 10 × 2.76 mm, 1.508 ct. Photos by Ludovica Faldi

appearance and show, in the half-sawed ones, a rim of a more saturated blue color that can already be seen with the naked eye. Some treated samples show a concentration of color along the fractures, not only confined to the fracture itself (as in the case of dyed samples) but also expanding on either side of the break. This color concentration, as well as the gem color itself, is rather unnatural to our experience and results from a treatment to improve the color in agreement with Fritsch et al. (1999).

Chemical analyses

The chemical analyses of natural and treated samples were performed on several points and lines from rim to center or from rim to rim. In natural gems, the compositions of different points resulted very similar and in agreement with the stoichiometric formula of turquoise (Table 1). As usual in the turquoise matrix, pyrite and kaolinite have been detected as accessory minerals.

The treated samples show high amounts of K due to the Zachery process and stoichiometric recalculation does not match the turquoise formula (Table 2). Moreover, significant contents of Na₂O also occur linearly correlated with K₂O (Fig. 2a). In the perpendicularly cut samples (*TT_7* and *TT_8*) the highest values of K and Na are found in the darker zones, well visible to the naked eye, and at the rim where an increase of P and a decrease of Al occur; an example of *TT_8* line 2 is given in Fig. 2b. In the inner parts of both samples, backscattered images evidence brighter areas enriched in CuO from 8 up to 29 wt% (an example of *TT_7* in Fig. 3 and chemical analyses in Table 3).

Table 1 Electron microprobe analyses of natural turquoises

Sample	TN_6		TN_7		TN_8	
	Average 31 pts	st dev	Average 31 pts	st dev	Average 31 pts	st dev
P ₂ O ₅ (wt%)	33.61	0.48	34.31	0.45	33.78	0.55
SiO ₂	0.01	0.02	0.02	0.02	0.05	0.03
Al ₂ O ₃	35.27	0.21	36.75	0.20	34.63	0.61
Fe ₂ O ₃	2.26	0.09	1.20	0.07	1.54	0.07
CuO	7.98	0.16	8.16	0.14	8.71	0.46
ZnO	0.03	0.04	0.08	0.07	0.04	0.04
CaO	0.06	0.02	0.05	0.01	0.07	0.05
Na ₂ O	0.02	0.02	0.01	0.02	0.01	0.01
K ₂ O	0.04	0.01	0.04	0.01	0.03	0.01
MgO	0.01	0.01	0.01	0.01	0.01	0.01
BaO	0.08	0.04	0.05	0.04	0.07	0.04
PbO	0.03	0.03	0.03	0.04	0.03	0.04
SO ₃	0.36	0.07	0.26	0.06	0.49	0.22
Total	79.77		80.96		79.44	
Structural formula based on 20 anions						
P	3.970		3.977		4.006	
Si	0.003		0.004		0.010	
Al	5.799		5.930		5.718	
Fe ³⁺	0.237		0.124		0.162	
Cu	0.836		0.839		0.915	
Zn	0.001		0.003		0.001	
Ca	0.007		0.005		0.007	
Na	0.002		0.002		0.001	
K	0.008		0.008		0.008	
Mg	0.001		0.001		0.001	
Ba	0.008		0.005		0.007	
Pb	0.004		0.004		0.004	
S	0.051		0.035		0.068	
Σ	10.927		10.937		10.909	
Cu + K + Na + Ba	0.86		0.86		0.93	
Al + Fe ³⁺	6.04		6.05		5.88	
P + Si + S	3.98		3.99		4.03	

310 In *TT_9*, analyzed from rim to rim only on the polished
 311 surface, the chemical composition respects the stoichiometry
 312 of turquoise except at the rims where contents of the
 313 K and Na oxides were higher (up to 3.8 and up to 0.5 wt%,
 314 respectively).

315 In general, the EDS analyses of our turquoises, both natural
 316 and treated, yielded results well in the range of those
 317 from WDS-EMP. In the treated samples, the highest Cu
 318 values were detected in the more brilliant white points that
 319 contain up to 34 wt% of CuO (an example, *TT_12*, Fig. 4).
 320 The rounded crystals show a pseudo-turquoise composition
 321 with a K₂O content up to 11 wt%; the platy area shows to
 322 be composed of both pseudo-turquoise and mixed phases
 323 with variable composition containing P, Si, K, Al, Mg, Na,
 324 Cu and Fe.

In addition, the core of *TT_12* (Fig. 4) displays on the
 325 central part of the sample, the presence of K-feldspar with
 326 composition: K_{0.98}Na_{0.03}Al_{1.0}Si_{2.93}O₈. In Fig. 5, a BSE
 327 image of the analyzed zone is displayed together with the
 328 X-ray maps of major elements. The feldspar (black star in
 329 BSE image, Fig. 5) is in contact with “the turquoise” where
 330 a 32 wt% CuO content was detected (red star in figure).
 331

An inspection at higher magnification of backscattered
 332 images evidenced white areas (Fig. 6) associated with white
 333 rounded “seeds” distributed around them (Fig. 6a–c) also
 334 visible in the near platy zone (Fig. 6d). The chemical compositions
 335 of the points labeled in Fig. 6 are listed in Table 4; the
 336 copper content is very high while aluminum and potassium
 337 contents are low (point 13). Moving away, the Cu content
 338 decreases whereas that of Al and K increases.
 339

Table 2 Representative electron microprobe analyses of treated turquoises

Sample	TT_7 line 1		TT_8 line 2				TT_9 line 1				
	rim	inter	rim	inter	inter	center	rim	inter	center	inter	rim
P ₂ O ₅ (wt%)	38.18	37.14	35.44	34.15	34.29	33.59	32.41	34.16	33.98	34.23	33.39
SiO ₂	0.05	0.02	0.03	0.05	0.01	0.04	0.08	0.03	0.02	–	–
Al ₂ O ₃	24.48	27.87	28.57	30.11	31.21	31.28	32.62	34.68	34.76	35.04	34.59
Fe ₂ O ₃	0.40	0.52	0.85	0.95	0.74	0.86	0.48	0.52	0.56	0.50	0.42
CuO	4.20	5.29	5.75	6.12	6.39	6.68	6.35	6.66	6.45	6.57	6.55
ZnO	0.02	0.03	0.21	0.18	0.32	0.21	0.05	0.03	–	0.03	0.11
CaO	0.66	0.14	0.16	0.10	0.18	0.34	0.06	0.08	0.02	0.06	0.07
Na ₂ O	2.14	1.61	0.88	0.70	0.53	0.30	0.50	0.25	0.20	0.22	0.36
K ₂ O	11.03	7.45	6.22	5.60	4.13	3.47	3.80	0.81	0.75	1.02	2.00
MgO	0.13	–	0.04	–	0.05	0.06	0.02	0.02	–	–	0.01
BaO	0.10	0.01	0.03	–	–	0.03	0.05	0.07	–	0.02	0.01
PbO	0.06	–	–	0.06	0.01	0.10	–	0.02	–	0.01	0.09
SO ₃	0.12	0.21	0.15	0.30	0.21	0.21	0.30	0.35	0.33	0.26	0.28
Total	81.57	80.28	78.33	78.32	78.07	77.15	76.73	77.69	77.08	77.96	77.88
Structural formula based on 20 anions											
P	4.611	4.459	4.361	4.197	4.199	4.158	4.021	4.090	4.088	4.087	4.031
Si	0.010	0.003	0.007	0.010	0.001	0.008	0.017	0.007	0.004	–	–
Al	4.115	4.659	4.894	5.152	5.321	5.390	5.634	5.780	5.822	5.824	5.813
Fe ³⁺	0.043	0.056	0.093	0.103	0.081	0.094	0.053	0.055	0.060	0.053	0.045
Cu	0.450	0.563	0.627	0.667	0.694	0.733	0.698	0.707	0.688	0.695	0.701
Zn	0.001	0.001	0.008	0.007	0.012	0.008	0.002	0.001	–	0.001	0.004
Ca	0.071	0.015	0.018	0.011	0.020	0.038	0.007	0.009	0.002	0.007	0.008
Na	0.296	0.222	0.124	0.099	0.074	0.042	0.072	0.034	0.027	0.030	0.050
K	2.631	1.767	1.512	1.360	0.999	0.849	0.931	0.192	0.179	0.241	0.477
Mg	0.012	–	0.003	–	0.005	0.005	0.002	0.002	–	–	0.001
Ba	0.011	0.001	0.003	–	–	0.003	0.005	0.008	–	0.002	0.001
Pb	0.010	–	–	0.009	0.002	0.016	–	0.003	–	0.001	0.014
S	0.017	0.029	0.021	0.044	0.030	0.031	0.044	0.050	0.047	0.037	0.039
Σ	12.277	11.775	11.672	11.659	11.438	11.375	11.486	10.937	10.918	10.978	11.184
Cu + K + Na + Ba	3.47	2.57	2.30	2.14	1.80	1.68	1.72	0.95	0.90	0.98	1.24
Al + Fe ³⁺	4.16	4.71	4.99	5.25	5.40	5.48	5.69	5.84	5.88	5.88	5.86
P + Si + S	4.64	4.49	4.39	4.25	4.23	4.20	4.08	4.15	4.14	4.12	4.07

340 Moreover, in sample *TT_11* (Fig. 7), SE images at very
 341 high magnification of the inner part of pores allow noting
 342 the growth of crystals that are similar to those identified
 343 as turquoises by Kwon et al. (2009) in Zachery-treated
 344 stones. These Authors suggest that the crystals filling the
 345 pores influence the stability and durability of the turquoise.
 346 Unfortunately, in our sample, the gold coating prevented the
 347 EDS analysis.

348 **X-ray powder diffraction**

349 Figure 8 shows a comparison between the XRPD pat-
 350 terns of (a) natural sample *TN_12*, (b) light blue in color
 351 inner part and (c) bluest in the color outer part of treated
 352 sample *TT_23*. All samples showed the characteristic

353 diffraction pattern of turquoise even though the treated
 354 turquoise exhibits larger unit cell parameters giving rise to
 355 a slight expansion of the unit cell volume when compared
 356 to the natural ones (461.88 vs. 461.44 Å³, respectively).
 357 The Rietveld analysis yields minor contents of pyrite (4
 358 wt%) in the natural sample whereas a 3 wt% of tenorite
 359 is obtained for the light blue area of the treated stones
 360 (Fig. 9).

361 Concerning the bluest area of the outer part of the
 362 treated sample, the XRPD pattern supports the existence
 363 of an amorphous phase that is clearly displayed by a diffuse
 364 bump in the 20–30 2θ° region of the background, suggest-
 365 ing the occurrence of a poor to non-crystalline phase in the
 366 outer part of the treated gem. Additionally, the lower size of
 367 the diffraction domains extracted from the microstructural

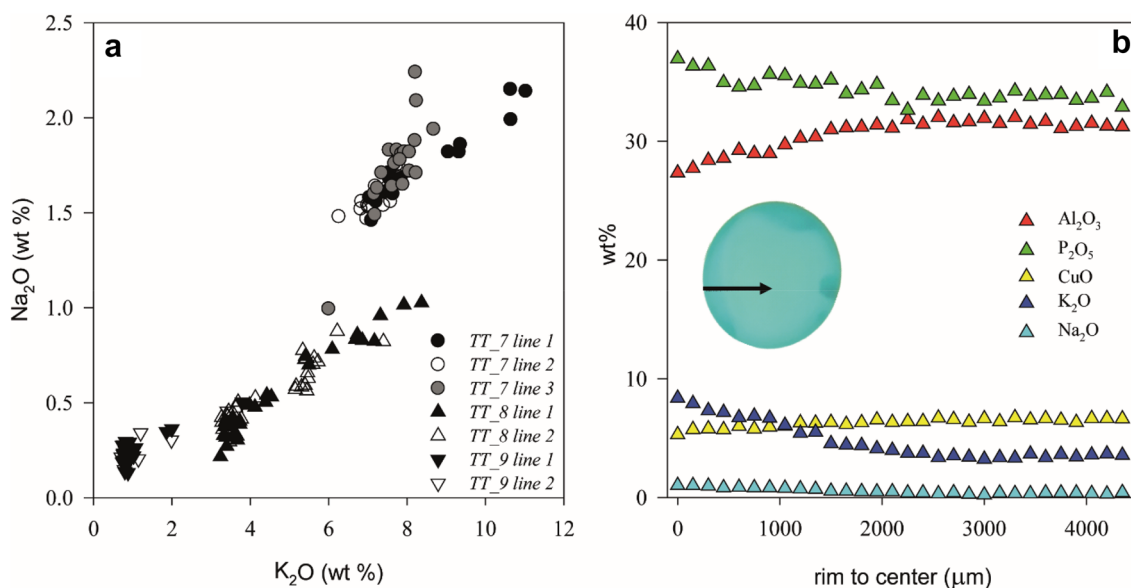


Fig. 2 a Variation of K₂O versus Na₂O of treated samples; b variation of different oxides in *TT_8 line 1* from rim to core

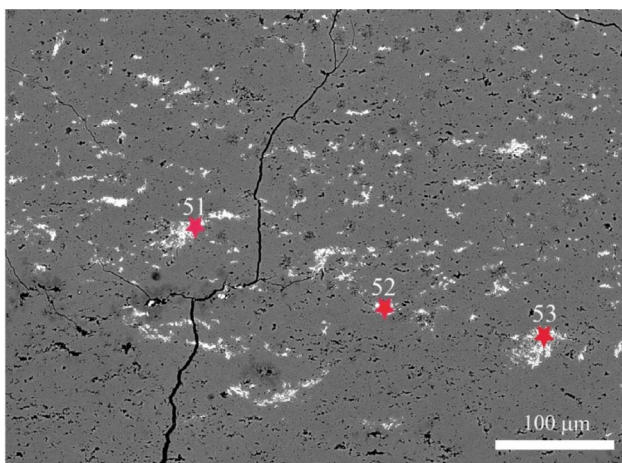


Fig. 3 BSE image of *TT_10* showing analyzed points reported in Table 3

Table 3 Electron microprobe analyses of points shown in Fig. 3

wt%	<i>TT_10</i>		
	51	52	53
P ₂ O ₅	35.78	33.90	36.01
SiO ₂	0.11	0.11	0.04
Al ₂ O ₃	12.45	7.11	16.19
Fe ₂ O ₃	0.23	0.21	0.31
CuO	24.17	28.96	19.36
ZnO	0.13	–	–
CaO	0.19	0.20	0.22
Na ₂ O	5.33	6.36	4.43
K ₂ O	5.73	4.63	6.40
MgO	–	0.02	0.03
BaO	0.02	0.08	0.08
PbO	–	–	0.03
SO ₃	0.03	0.05	0.03
Total	84.16	81.63	83.12

368 analysis suggests a poor crystallinity of this material occur-
 369 ring in the outer layer of the gem.

370 **Laboratory-based X-ray Computed**
 371 **microtomography (μCT)**

372 The μCT analyses allowed exploring in a non-invasive way
 373 the microstructure of natural (*TN_11*) and treated (*TT_20*)
 374 gems. The former is characterized by an outer surface with
 375 micropores and microcracks leading to a whole porosity of
 376 5 vol% (Fig. 10a). These cracks do not show any preferred
 377 orientation and develop also in the inner part of the gem
 378 and appear filled with finely aggregates characterized by

high and low grey scale values (Fig. 10b, c). The EMPA
 analyses of the same sample suggest the occurrence of clay
 minerals and pyrite filling the cracks.

In Fig. 11a, the volume rendering of the treated gem
 is displayed, and a reconstructed axial slice of its inner
 part is shown in Fig. 11b. It is clear that surface porosity
 observed in natural samples is now completely lost
 whereas the outer white circular region (i.e., with the high-
 est attenuation of X-rays) appears and extends in its inner
 part exhibiting a concentric banding. In the core of the
 gem, well-rounded aggregates with high grey scale values
 appear randomly dispersed and exhibit a size of ~ 20 μm

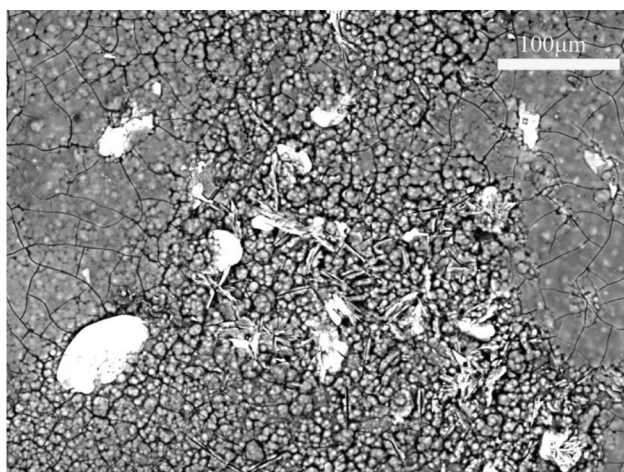


Fig. 4 BSE image of *TT_12*

(Fig. 11c). 3D rendering of the segmented highly absorbing aggregates is shown in Fig. 11d.

Fourier transform infrared spectroscopy

FTIR and ER-FTIR spectra of natural and treated turquoises were collected on several points and traverses from the rim to the center of the samples. It is noteworthy that FTIR

requires a microsampling, which may not be routinely carried out in the analysis of gems whereas ER-FTIR allows for a non-invasive investigation of the surface of materials, which potentially opens its use for gemological applications. As a drawback, intrinsic limitations of this last technique include the possible presence of spectral artifacts due to surface effects and the need for reference data for spectral interpretation.

Selected results are given in Figs. 12 and 13. Both IR techniques show slight differences in the patterns collected on natural and treated turquoises.

In the water stretching region (4000–2700 cm^{-1}), the FTIR spectra of our natural untreated samples (pattern a, Fig. 12) show peaks at 3509, 3466, 3453, 3293 and 3078 cm^{-1} that are due to the OH/H₂O vibrations (Abdu et al. 2011; Čejka et al. 2015), while the ER-FTIR spectra (patterns a, Fig. 13) show sharp peaks at 3497, 3461, 3438 cm^{-1} and broad bands at 3225 and 3031 cm^{-1} due to hydroxyl groups and to the two independent water units in the turquoise structure, respectively (Reddy et al. 2006; Abdu et al. 2011; Schwarzingler and Schwarzingler 2017; Sabbaghi 2018). The stretching and bending vibrations of PO₄ units are located between 1200 and 400 cm^{-1} . The main bands are found at 1107, 1058, 608, and 550 cm^{-1} in the FTIR spectra (pattern a, Fig. 12) and at 1118, 1049 and 1006 cm^{-1} and 834 cm^{-1} in the ER-FTIR ones in Fig. 13,

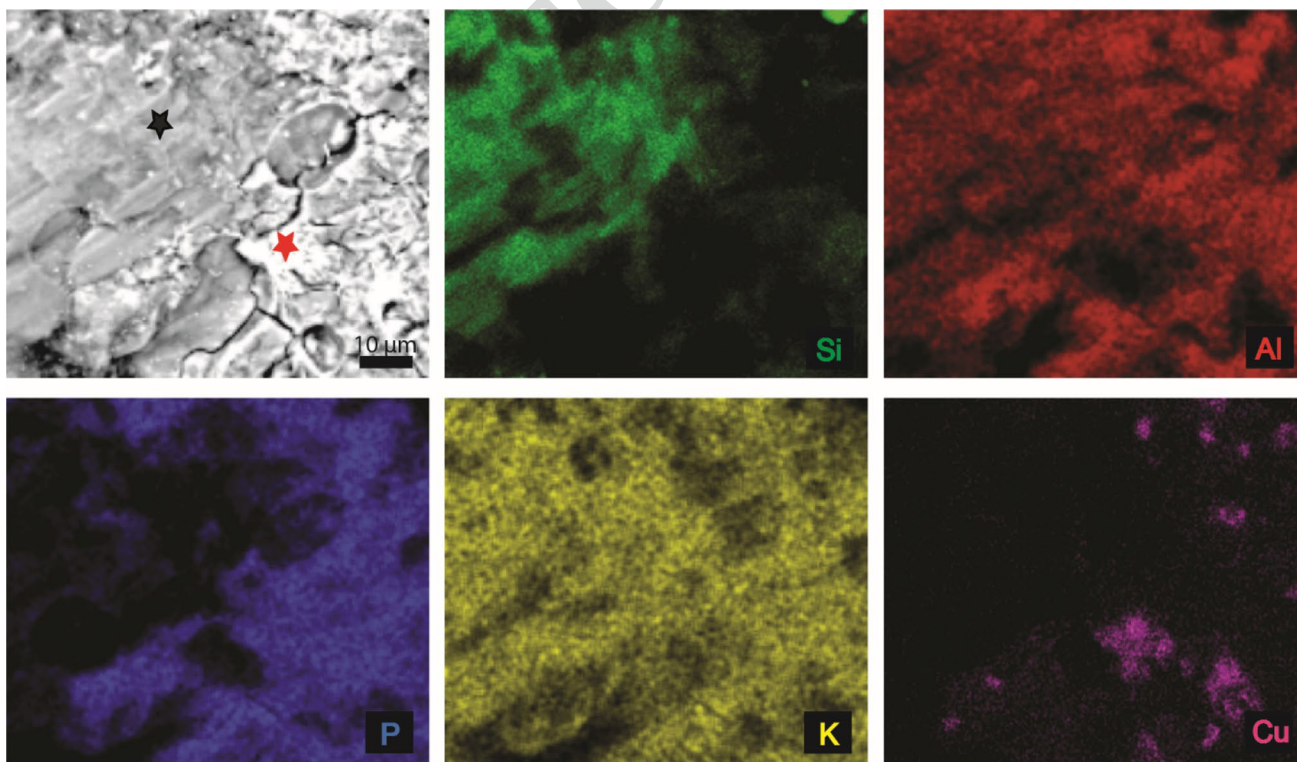


Fig. 5 BSE image and X-ray maps of selected elements of *TT_12*

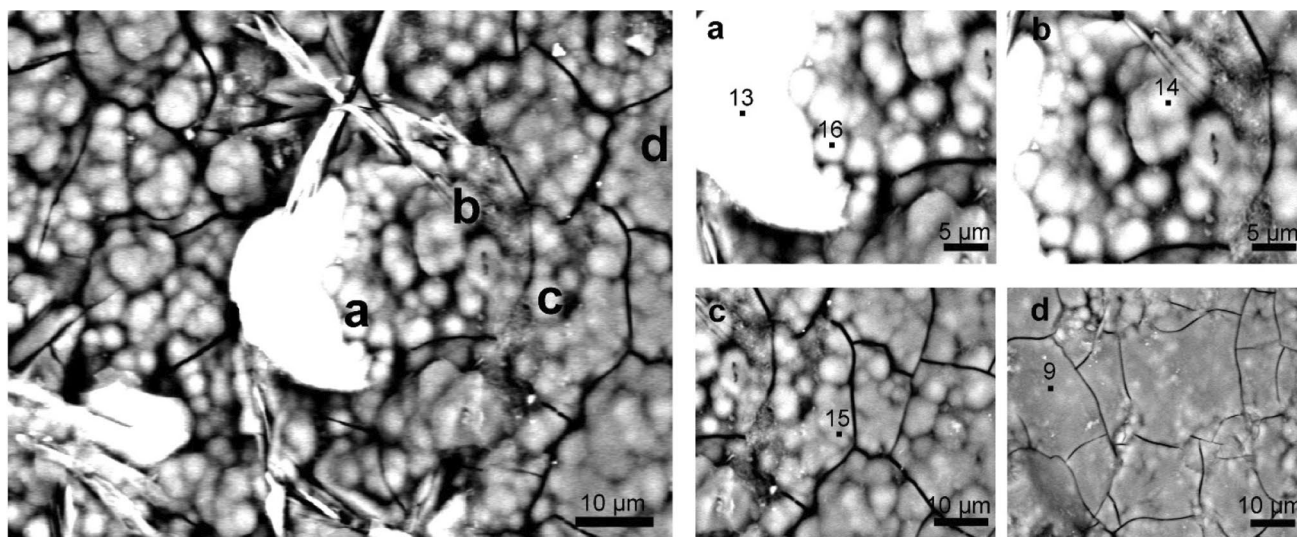


Fig. 6 BSE images of TT_12, on the left, and enlargements of the indicated a, b, c, d areas showing the analyzed points reported in Table 4, on the right

Table 4 EDS chemical analyses of points shown in Fig. 6

	TT_12				
	13	16	14	15	9
P ₂ O ₅ (wt%)	37.79	33.35	34.14	38.38	32.8
SiO ₂	1.05	0.92	0.84	0.98	3.49
Al ₂ O ₃	2.95	15.54	17.42	18.09	18.43
CuO	34.47	6.53	3.38	3.5	3.37
CaO	–	3.41	4.31	5.22	–
Na ₂ O	–	2.12	1.43	0.98	1.59
K ₂ O	4.7	7.81	8.49	9.58	8.66
Total	80.96	69.68	70.01	76.73	68.34

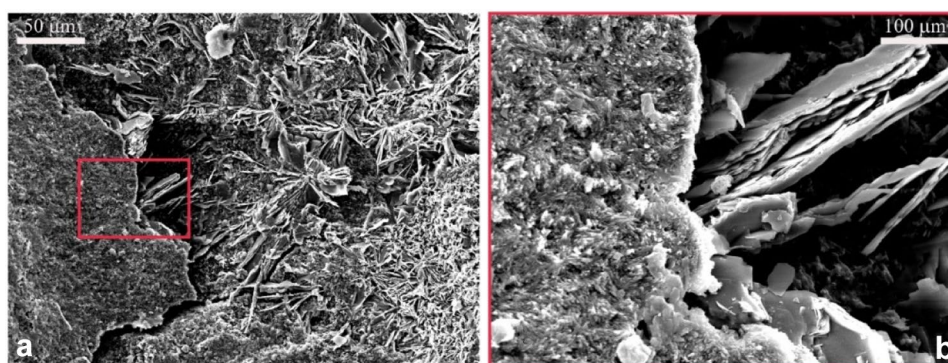
423 pattern a (Fritch et al. 1999). These FTIR and ER-FTIR
 424 spectral features are well distinctive of crystalline natural
 425 turquoise.

426 At least two new components at about 3380 cm⁻¹ and
 427 3600 cm⁻¹ appear in the FTIR spectra of treated samples

(arrowed in pattern b of TT_24 as an example, Fig. 12);
 the former strongly overlaps with the 3280 cm⁻¹ broad
 component, while the latter appears as a strong asym-
 metry of the 3509 cm⁻¹ band. Slight modifications of
 the FTIR patterns are also visible in the range of PO₄
 antisymmetric stretching modes (1200–1000 cm⁻¹:
 Ross 1974; Della Ventura et al. 2019), where shifts and
 broadening of the 1188–1160 cm⁻¹ peaks are observed
 in treated turquoises (pattern b of TT_24 as an example,
 Fig. 12).

Differences in terms of relative intensities, position
 and width of bands are clearly visible in the ER-FTIR
 spectra of treated turquoises. In particular, the OH/H₂O
 stretching bands of structural water appear weaker and
 less defined than in the ER-FTIR spectra of natural ones
 (pattern b, Fig. 13). The bands in the PO₄ stretching region
 are broader, the main peak of turquoise shifts from 1118 to
 1111 cm⁻¹, and some bands (i.e., at 1158 cm⁻¹) disappear
 whereas the bands at 2958, 2917 and 2848 cm⁻¹ (–CH₂

Fig. 7 a SE images of TT_11; b zooming of red rectangle in (a)



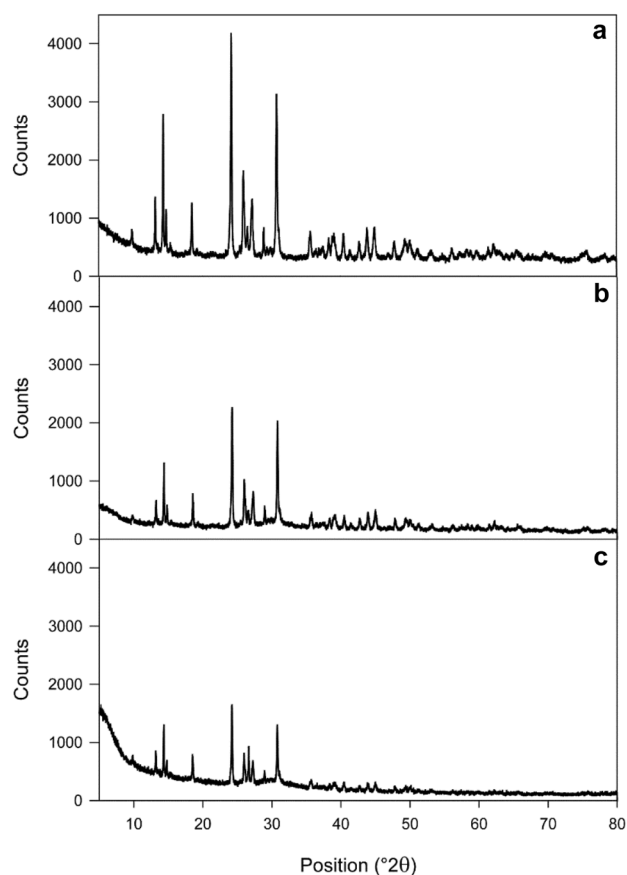
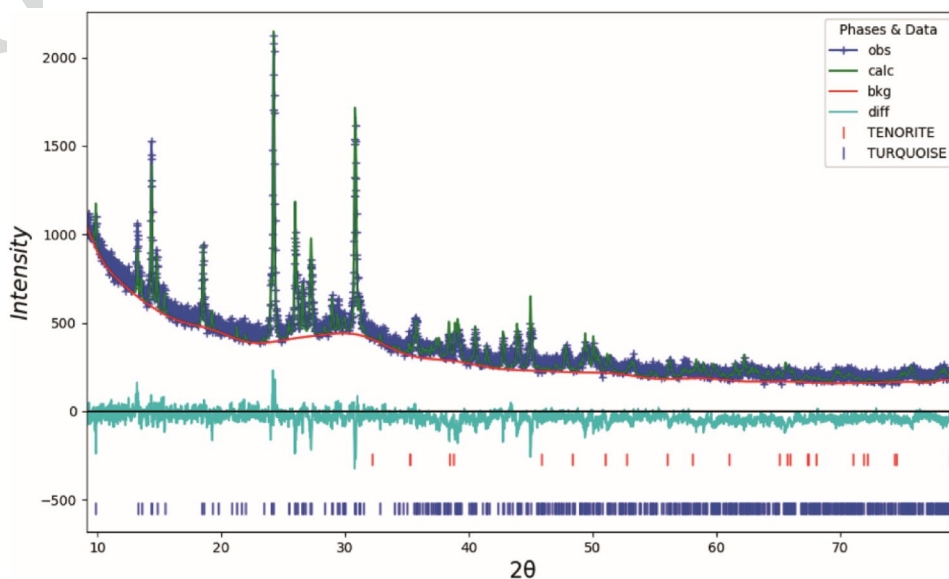


Fig. 8 XRPD patterns of a) *TN_12*, b) inner and c) outer part of *TT_23*

and $-\text{CH}_3$ stretching vibrations) (pattern b, Fig. 13) are due to wax used to polish the surface of the treated turquoise (Han et al. 2015).

Fig. 9 Observed and calculated X-ray powder diffraction pattern after the Rietveld refinement of sample *TT_23*



In the core of the treated gems, the possible structural/compositional variations are less evident and the ER-FTIR spectra resemble those of the untreated natural well-crystalline turquoise (e.g., pattern c, Fig. 13).

A completely different vibrational pattern is obtained in correspondence with the internal rims and of crystal aggregates randomly dispersed in the core of the gem already analyzed by micro-tomography *TT_20* (the same particles having high grey scale values and micrometric size in the micro-CT analyses of Fig. 9). In these regions (see pattern d, Fig. 13), strong reflectance peaks at 1101, 1073, 995 cm^{-1} and weaker peaks at 1208, 1166, 912, 858 cm^{-1} are due to an unidentified crystalline phase. This spectrum is compatible with that of a hydroxide (maybe a potassium-containing phase) and/or of alumina (Schroeder 2002; Hosseini et al. 2011; Hong et al. 2016; Schwarzingler and Schwarzingler 2017; Sabbaghi 2018) but further investigations in reflectance mode on mineral references would be needed for its/their unambiguous identification.

Discussion and conclusions

In this study, a multidisciplinary approach offers significant novel insight into the undisclosed property Zachery treatment on turquoise. The comparison between natural and treated turquoise allows identifying, for the first time, new chemical–mineralogical and microstructural features, which are distinctive of the Zachery treatment and will be hereafter discussed.

- Chemical analyses performed by EMPA on treated samples confirmed the presence of K as already reported in the literature (Fritsch et al. 1999; Kwon et al. 2009; Sun

Fig. 10 Natural turquoise *TN_11*: **a** 3D volume rendering (200×500×1000 voxels); **b** selected sagittal reconstructed slice; **c** minerals filling fractures (zooming of the red rectangle in **b**)

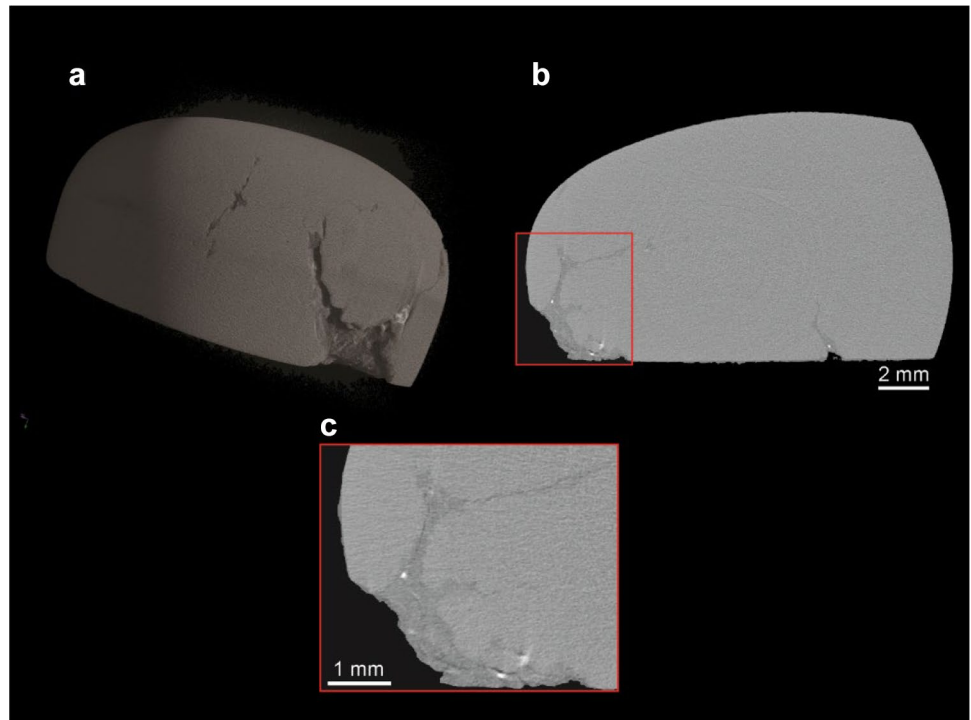
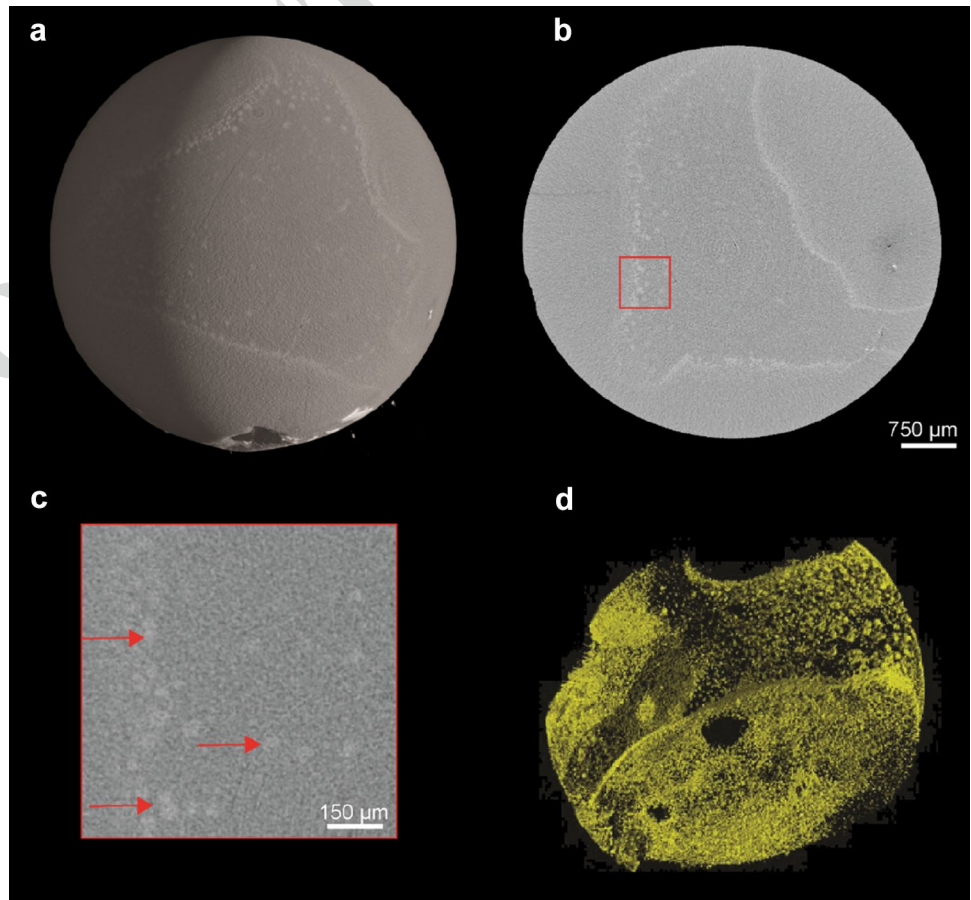


Fig. 11 Zachery treated turquoise *TT_20*: **a** 3D volume rendering (500×500×500 voxels); **b** selected axial reconstructed slice; **c** rounded highly X-ray attenuation aggregates (zooming of the red rectangle in fig. **b**); **d** 3D rendering of the segmented highly absorbing aggregates



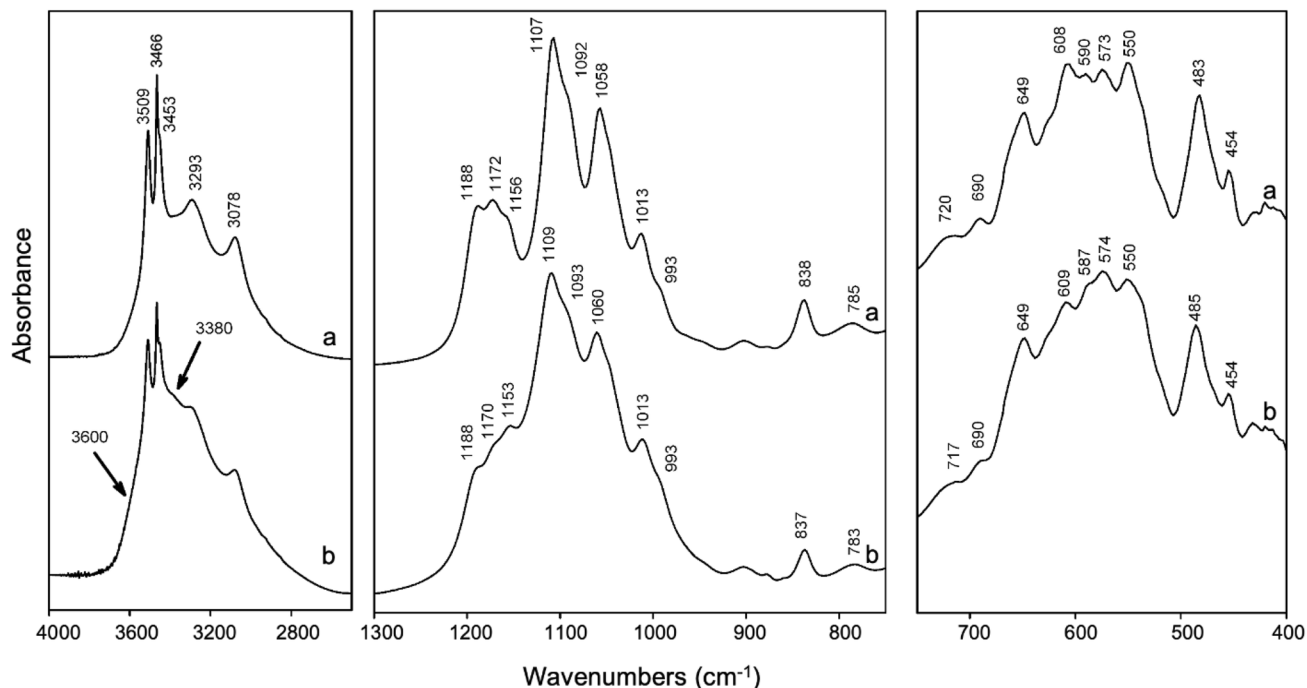


Fig. 12 FTIR spectra collected in the different wavenumber ranges: from 4000 to 2600 cm^{-1} (left panel), from 1300 to 750 cm^{-1} (center panel), and from 750 to 400 cm^{-1} (right panel). **a** Natural *TN_14* and **b** treated *TT_24* turquoise

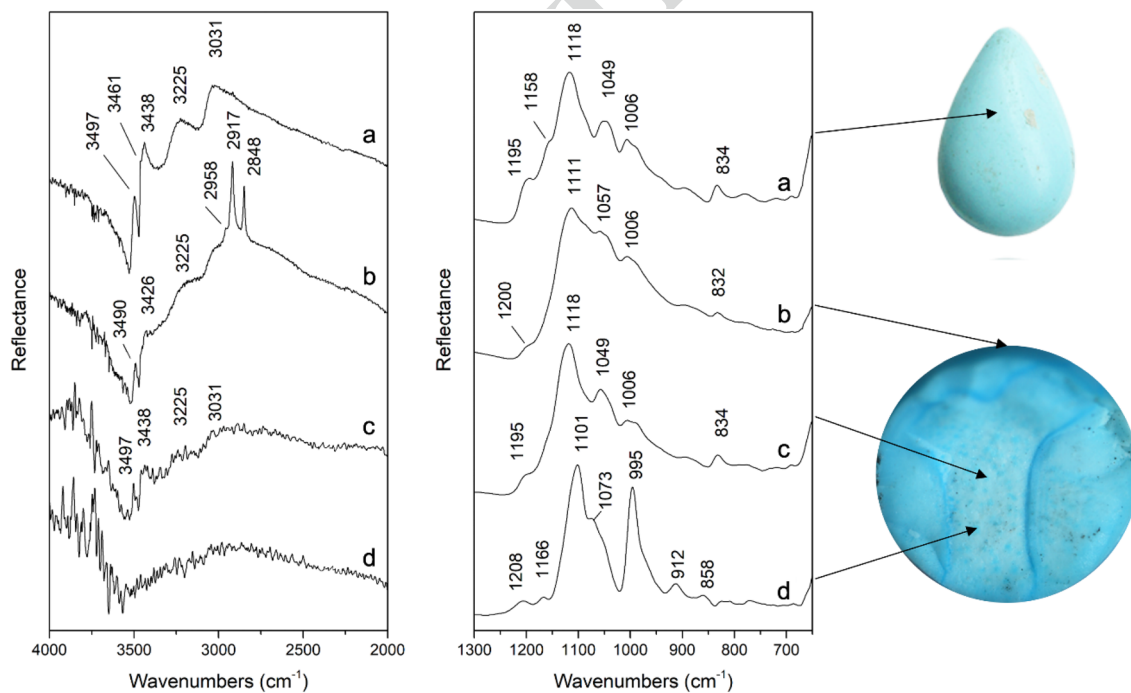


Fig. 13 ER-FTIR spectra collected in specular geometry on different wavenumber ranges: from 4000 to 2000 cm^{-1} (left panel) and from 1300 to 650 cm^{-1} (right panel). *TN_15* natural turquoise (**a**), *TT_20* treated turquoise in correspondence of the treated surface (**b**), of core of the gem (**c**) and of the bluish internal rims and bluish crystal aggregates randomly dispersed in the core of the gem (**d**)

et al. 2014) but pointed out new diagnostic chemical features for the treatment. The quantitative analysis by WDS highlights a variable composition overall in terms of minor oxides (mainly K and Na) in the treated turquoises that do not respect its stoichiometric formula. This suggests that a newly formed phase (“*transitional phase*”, see below), with a chemical composition close to the one of turquoise but not attributable to one of the six end members of its isostructural series (Abdu et al 2011), is the resulting product of the Zachery treatment. At present, no crystalline phases with a chemical composition matching the one calculated are available in the literature.

- The presence of K in treated samples well agrees with the hypothesis of Frisch et al. (1999) suggesting that turquoise grows in situ within the porous areas during the treatment process. The involvement of potassium in the formation of turquoise is also described in the recent paper on the Ali Abad Cu Porphyry Deposit in central Iran, by Ardekani et al. (2020). The Authors suggest that the presence of potassium in some analyses of turquoises probably indicates the presence of a *transitional phase* resulting from the conversion of sericite or alunite to turquoise and they report a series of reactions under acid conditions involving sulfates, phosphates, and potassium (released from the alteration of feldspars) finally bearing to the crystallization of turquoise;
- BSE images and EDS analyses highlight scattered spots yielded very high copper concentration up to 34 wt% CuO in the inner part of the treated turquoise and suggest that these Cu-rich areas are microspheres (“seeds”) that decrease in size and in copper content moving from the inner core to the outer part of the gem;
- EDS and XRPD analyses of treated samples highlighted the occurrence of K-feldspar and tenorite. The former should represent a relict of the “beds of feldspar” used during the Zachery process while the latter (CuO) can be interpreted as the product of the oxidation of copper sulfides added in the soaking process. We might suppose in the Zachery treatment the use of chemicals such as copper sulfate for the enhancement of turquoise. As noticed for chalcedony by Koivula and Kammerling (1989), man-made “inclusions” may be produced by soaking porous samples in a copper solution and then applying an electric current to precipitate out a dendrite of elemental copper;
- The XRPD patterns suggest that the outer surface of the treated turquoise is characterised by the coexistence of a crystalline phase, namely turquoise, with an amorphous/poorly crystalline phase (probably the transitional phase and/or the residues of the products used in the treatment). Furthermore, the structural refinement of the turquoise on the gem surface indicates a

lower crystallinity. The hypothesis is that the Zachery treatment induces the re-crystallization of a new turquoise which differs from the natural one from a microstructural point of view;

- X-ray computed microtomography allows investigating of both the outer and inner part of the gem in a totally non-invasive way; the effects of the Zachery treatment are clearly observable not only on the surface but also in its inner core. Concentric banding associated with well-rounded aggregates (CuO seeds) extends from the inner to the outer surface. Furthermore, the enhancement due to the treatment resulted in a lowering of the value of porosity in treated samples which may justify the darker surface color of treated samples;
- The spectral differences detected by the two infrared techniques (FTIR and ER-FTIR) suggest the occurrence of possible structural and/or compositional slight variations between natural and treated turquoise, thus confirming the XRPD results. This spectral modification is detectable on the external surface of treated turquoises as well as in the subsurface regions of the treated gem (as showed by ER-FTIR spectra collected on the internal rims of cross-sectioned samples) and suggests a surface-bulk gradient of the effects induced by the Zachery method.

In conclusion, we might assert that the combination of several analytical techniques allows for the complete characterization of natural and treated turquoise, thus providing (i) new chemical and structural features, which are peculiar to the Zachery treatment and (ii) new insights into this turquoise treatment. In particular, the non-destructive ER-FTIR spectroscopy and microtomography allow distinguishing, in a fast and easy way, between natural and Zachery-treated samples whereas invasive EMPA-EDS and XRPD can provide information on the treatment process.

Acknowledgements The authors gratefully thank Claudio Cimmino, Bangkok, Thailandia for providing the samples here investigated, Giada Marchetti for collecting part of the experimental data during her degree and Ludovica Faldi (IGI Milan) for acquiring the gem photos.

Author contributions VD, NM and RB wrote the main manuscript text. VD performed the EMP analysis and interpreted the results. EP, NM and GDV performed the FT-IR analysis and elaborated on the data. NM and MC performed XRPD and elaborated on the data. IA performed the gemological analyses. LM performed the X-ray computed microtomography analysis and LM and NM elaborated the data. All authors assisted in the revision of the initial draft of the manuscript.

Funding The authors did not receive support from any organization for the submitted work.

Declarations

Conflict of interest The authors declare no competing interests. The authors have no relevant financial or non-financial interests to disclose.

584 **References**

585 Abdu YA, Hull SK, Fayek M, Hawthorne FC (2011) The turquoise-
586 chalcocopper Cu(AlFe³⁺)₆(PO₄)₄(OH)₈·4H₂O solid-solution
587 series: A Mössbauer spectroscopy, XRD, EMPA, and FTIR
588 study. *Am Mineral* 96:1433–1442. [https://doi.org/10.2138/am.
589 2011.3658](https://doi.org/10.2138/am.2011.3658)

590 Ardekani SJ, Mackizadeh MA, Ayati F (2020) Mineralogy and forma-
591 tion conditions of turquoise in Ali Abad Cu Porphyry deposit. *J*
592 *Econ Geol* 12(1):93–109. [https://doi.org/10.22067/econg.v12i1.
593 72122](https://doi.org/10.22067/econg.v12i1.72122)

594 Carò F, Schorsch D, Smieska L, Santarelli B (2021) Non-invasive XRF
595 analysis of ancient Egyptian and near Eastern turquoise: a pilot
596 study. *Archaeol Sci Rep* 36:102893. [https://doi.org/10.1016/j.
597 jasrep.2021.102893](https://doi.org/10.1016/j.jasrep.2021.102893)

598 Caruso V, Marinoni N, Diella V, Berna F, Cantaluppi M, Mancini
599 L, Trombino L, Cattaneo C, Pastero L, Pavese A (2020) Bone
600 diagenesis in archaeological and contemporary human remains:
601 an investigation of bone 3D microstructure and mineral-chemical
602 assessment. *Archaeol Anthropol Sci* 12:1–18. [https://doi.org/10.
603 1007/s12520-020-01090-6](https://doi.org/10.1007/s12520-020-01090-6)

604 Čejka J, Sejkora J, Macek I, Malíkova R, Wang L, Scholz R, Xi Y,
605 Frost RL (2015) Raman and infrared spectroscopic study of tur-
606 quoise minerals. *Spect Acta Part A* 149:173–182. [https://doi.org/
607 10.1016/j.saa.2015.04.029](https://doi.org/10.1016/j.saa.2015.04.029)

608 Della Ventura G, Capitelli F, Capitani G, Ventruti G, Monno A
609 (2019) X-ray structure refinement and vibrational spectroscopy
610 of metauxite FeAl₂(PO₄)₂(OH)₂·8H₂O. *Crystals* 9(297):1–14.
611 <https://doi.org/10.3390/cryst9060297>

612 Dumanska-Słowik M, Weselucha-Birczyńska A, Natkaniec-Nowak L,
613 Gawel Ł, Włodek A (2020) blue or green? Turquoise-planerite
614 species from Carico Lake Valley in Nevada, the United States: evi-
615 dence from Raman spectroscopy. *J Raman Spectrosc* 51:346–356.
616 <https://doi.org/10.1002/jrs.5761>

617 Feldkamp LA, Davis LC, Kress JW (1984) Practical cone-beam
618 algorithm. *J Opt Soc Am A* 1:612–619. [https://doi.org/10.1364/
619 JOSAA.1.000612](https://doi.org/10.1364/JOSAA.1.000612)

620 Fritsch E, Rondeau B (2009) Gemology: the developing science of
621 gems. *Elements* 5:147–152. [https://doi.org/10.2113/gselements.5.
622 3.147](https://doi.org/10.2113/gselements.5.3.147)

623 Fritsch E, McClure SF, Ostrooumov M, Andres Y, Moses T, Koivula
624 JI, Kammerling RC (1999) The identification of Zachery-treated
625 turquoise. *Gems Gemol* 35:4–16

626 Hainschwang T, Notari F (2008) Specular reflectance infrared spectro-
627 scopy—a review and update of a little exploited method for gem
628 identification. *J Gemmol* 31:23–29

629 Han W, Lu T, Dai H, Su J, Dai H (2015) Impregnated and dyed tur-
630 quoise. *Gems Gemol* 51:343–345

631 Hole F, Flannery KV, Neely JA (1969) Prehistory and human ecology
632 of the deh luran plain: an early village sequence from Khuzistan,
633 Iran. University of Michigan Press. [https://doi.org/10.3998/mpub.
634 11395036](https://doi.org/10.3998/mpub.11395036)

635 Hong Z, Li J, Jiang J, Li Z, Xu R (2016) Competition between bacteria
636 and phosphate for adsorption sites on gibbsite: an in-situ ATR-
637 FTIR spectroscopic and macroscopic study. *Colloids Surfaces B*
638 148:496–502. <https://doi.org/10.1016/j.colsurfb.2016.09.026>

639 Hosseini SA, Niaei A, Salari D (2011) Production of γ-Al₂O₃ from
640 Kaolin. *Open J Phys Chem* 1:23–27. [https://doi.org/10.4236/ojpc.
641 2011.12004](https://doi.org/10.4236/ojpc.2011.12004)

642 Koivula JI, Kammerling RC (1989) Gems news. *Gems Gemol*
643 25:45–51

Kudrna Prašek M, Pistone M, Baker DR, Sodini N, Marinoni N, Lan-
zafame G, Mancini L (2018) A compact and flexible induction
furnace for in situ X-ray microradiography and computed micro-
tomography at Elettra: design, characterization and first tests. *J*
Synchrotron Rad 25(4):1172–1181. [https://doi.org/10.1107/S1600
577518005970](https://doi.org/10.1107/S1600577518005970)

Kwon KR, Bang SY, Park JW, Shim KB (2009) Structural charac-
teristics of Zachery-treated turquoise. *J Korean Cry Growth Cry*
Tech 19:95–101

Lind T, Schmetzer K, Bank H (1983) The identification of turquoise by
infrared spectroscopy and X-ray powder diffraction. *Gems Gemol*
19:164–168

Mancini L, Dreossi D, Fava C, Sodini N, Tromba G (2007) TomoLab:
the new X-ray micro-tomography facility at Elettra. *Elettra High-*
lights 2006–2007

McClure SF, Kane RE, Sturman N (2010) Gemstones enhancement and
its detection in the 2000s. *Gems Gemol* 46:218–240

Reddy BJ, Frost RL, Weier ML, Martens WN (2006) Ultraviolet-
Visible, near infrared and mid infrared reflectance spectroscopy
of Turquoise. *J near Infr Spectr* 14:241–250. [https://doi.org/10.
1255/jnirs.641](https://doi.org/10.1255/jnirs.641)

Rietveld HM (1969) A profile refinement method for nuclear and mag-
netic structures. *J App Cryst* 2:65–71

Ross SD (1974) Phosphates and other oxy-anions of group V. In:
Farmer VC (ed) Mineralogical society monograph 4: the infrared
spectra of minerals. Mineralogical Society of Great Britain and
Ireland, Twickenham

Sabbaghi HA (2018) A combinative technique to recognise and dis-
criminate turquoise stone. *Vib Spec* 99:93–99. [https://doi.org/10.
1016/j.vibspec.2018.09.002](https://doi.org/10.1016/j.vibspec.2018.09.002)

Schindelin J, Arganda-Carreras I, Frise E et al (2012) Fiji: an open-
source platform for biological-image analysis. *Nat Methods*
9:676–682. <https://doi.org/10.1038/nmeth.2019>

Schroeder PA (2002) Infrared Spectroscopy in Clay Science. In: Rule
A, Guggenheim S (eds) CMS Workshop Lectures. Teaching Clay
Science 11: 181–206. <https://doi.org/10.1346/CMS-WLS-11.11>

Schwarzinger B, Schwarzinger C (2017) Investigation of turquoise
imitations and treatment with analytical pyrolysis and infrared
spectroscopy. *J Anal Appl Pyrolysis* 125:24–31. [https://doi.org/
10.1016/j.jaap.2017.05.002](https://doi.org/10.1016/j.jaap.2017.05.002)

Shigley JE, McClure SF (2009) Laboratory-treated gemstones. *Ele-*
ments 5:175–178. <https://doi.org/10.2113/gselements.5.3.175>

Sun LH, Ling A, Yu F, He Z, Ma W (2014) A tentative discussion on
Zachery-treated turquoise. *Acta Petr Miner* 33:165–171 (**in**
Chinese, abstract in English)

Toby BH, Dreele RB (2013) GSAS-II: the genesis of a modern open-
source all purpose crystallography software package. *J App Cryst*
46:544–549. <https://doi.org/10.1107/S002188981300353>

Zandomenighi D, Voltolini M, Mancini L, Brun F, Dreossi D, Pol-
acci M (2010) Quantitative analysis of X-ray microtomography
images of geomaterials: application to volcanic rocks. *Geosphere*
6:793–804. <https://doi.org/10.1130/GES00561.1>

Publisher's Note Springer Nature remains neutral with regard to jurisdictional claims in published maps and institutional affiliations.

Springer Nature or its licensor (e.g. a society or other partner) holds exclusive rights to this article under a publishing agreement with the author(s) or other rightsholder(s); author self-archiving of the accepted manuscript version of this article is solely governed by the terms of such publishing agreement and applicable law.

Journal:	269
Article:	1241

Author Query Form

Please ensure you fill out your response to the queries raised below and return this form along with your corrections

Dear Author

During the process of typesetting your article, the following queries have arisen. Please check your typeset proof carefully against the queries listed below and mark the necessary changes either directly on the proof/online grid or in the 'Author's response' area provided below

Query	Details Required	Author's Response
AQ1	Please confirm if the author names are presented accurately and in the correct sequence (given name, middle name/initial, family name). Author 6 Given name: [Giancarlo Della] Last name [Ventura]. Also, kindly confirm the details in the metadata are correct.	
AQ2	Inclusion of a data availability statement is preferred for this journal. If applicable, please provide one.	
AQ3	Please provide volume ID for reference [Mancini et al. 2007]	